Steel and Composite Structures, *Vol. 39, No. 3 (2021) 337-352*
DOI: https://doi.org/10.12989/scs.2021.39.3.337

Seismic behavior and strength of L-shaped steel reinforced concrete column-concrete beam planar and spatial joints

Zongping Chen*[1,2], Deyi Xu[1], Jinjun Xu[3] and Ni Wang[4]

[1]College of Civil Engineering and Architecture, Guangxi University, 100# east daxue road, Nanning,530004, China
[2]Key Laboratory of Disaster Prevention and Structure Safety of Chinese Ministry of Education, Guangxi University, 100# east daxue road, Nanning,530004, China
[3]College of Civil Engineering, Nanjing Tech University, No. 30, Puzhu South Road, Nanjing,211800, China
[4]College of Civil and Environment Engineering, Chang'an University, Middle section of South Second Ring Road, Xi'an,710064, China

(*Received June 17, 2020, Revised April 5, 2021, Accepted April 12, 2021*)

Abstract. The study presented experimental and numerical investigation on the seismic performance of steel reinforced concrete (SRC) L-shaped column- reinforced concrete (RC) beam joints. Various parameters described as steel configuration form, axial compressive ratio, loading angle, and the existence of slab were examined through 4 planar joints and 7 spatial joints. The characteristics of the load-displacement response included the bearing capacity, ductility, story drift ratio, energy-dissipating capacity, and stiffness degradation were analyzed. The results showed that shear failure and flexural failure in the beam tip were observed for planar joints and spatial joint, respectively. And RC joint with slab failed with the plastic hinge in the slab and bottom of the beam. The results indicated that hysteretic curves of spatial joints with solid-web steel were plumper than those with hollow-web specimens. The capacity of planar joints was higher than that of space joints, while the opposite was true for energy-dissipation capacity and ductility. The high compression ratio contributed to the increase in capacity and initial stiffness of the joint. The elastic and elastic-plastic story deformation capacity of L-shaped column frame joints satisfied the code requirement. A design formula of joint shear resistance based on the superposition theory and equilibrium plasticity truss model was proposed for engineering application.

Keywords: steel reinforced concrete; L-shaped column; planar joint; space joint; pseudo-static test; seismic behavior; loading angle; hysteretic performance

1. Introduction

Nowadays, with the increase of the urban population, more and more multi-story buildings were introduced to the community and business center. The columns with large sectional depth are needed to satisfy the requirement of the capacity, which leads the column protruding out of the wall. To meet the buyer's demand for more free space in the house and aesthetic demand the special-shaped column was adopted by the architects as a solution for the problems above. The special-shaped columns included L-shaped, T-shaped, and crisscross-shaped sections were suitably located in the corners as well as the intersection of structure, which have a promising prospect for frame structure.

Back in the past decades, many research about the specially shaped column had been conducted. In the early, most research had focused on the static behavior of the reinforced special-shaped concrete column (Marin 1979, Ramamurthy and Khan 1983, Thomas and M. ASCE 1985). Many computational methods were proposed to investigate the ultimate load, the interaction curves, and the relationship between the bending moment and curvature (Hsu 1989, Mahadevappa 1992, Dundar and Sahin 1993). In the 90s, it was of interest to investigate the seismic behavior of the special-shaped column, and plenty of experiments were conducted (Zhao *et al.* 2004, Cao *et al.* 2005). According to the above research, it was revealed that the cracking resistance and seismic performance of the special-shaped column are critical issues for the practical application. In accord with the current code (China 2006), the special-shaped RC column had a strict limitation in structural design. To improve the mechanical performance of the special-shaped column and extend its range of applications, SRC columns and concrete-filled steel tubular (CFT) special-shaped columns were employed to replace the RC column owing to its excellent performance, such as high stiffness and capacity, perfect durability, and good energy dissipation capacity. Many research had been conducted to demonstrate the performance of the SRC column. Mirza and Lacroix (2004) collected 150 physical tests of SRC columns and made a series of recommendations for ACI codes based on the comparative analysis on the strength. Xue *et al.* (2012) carried out experiments on the 17 SRC special-shaped column under cyclic lateral load and proposed a formula for the ultimate shear capacity of the composite columns. (Yang *et al.* 2015) performed an experimentally and numerically investigation on static behavior of T-shaped concrete-filled steel tubular (CFST) columns. These results indicated that both the two

*Corresponding author, Professor
E-mail: zpchen@gxu.edu.cn

http://www.techno-press.org/?journal=scs&subpage=8
ISSN: 1229-9367 (Print), 1598-6233 (Online)

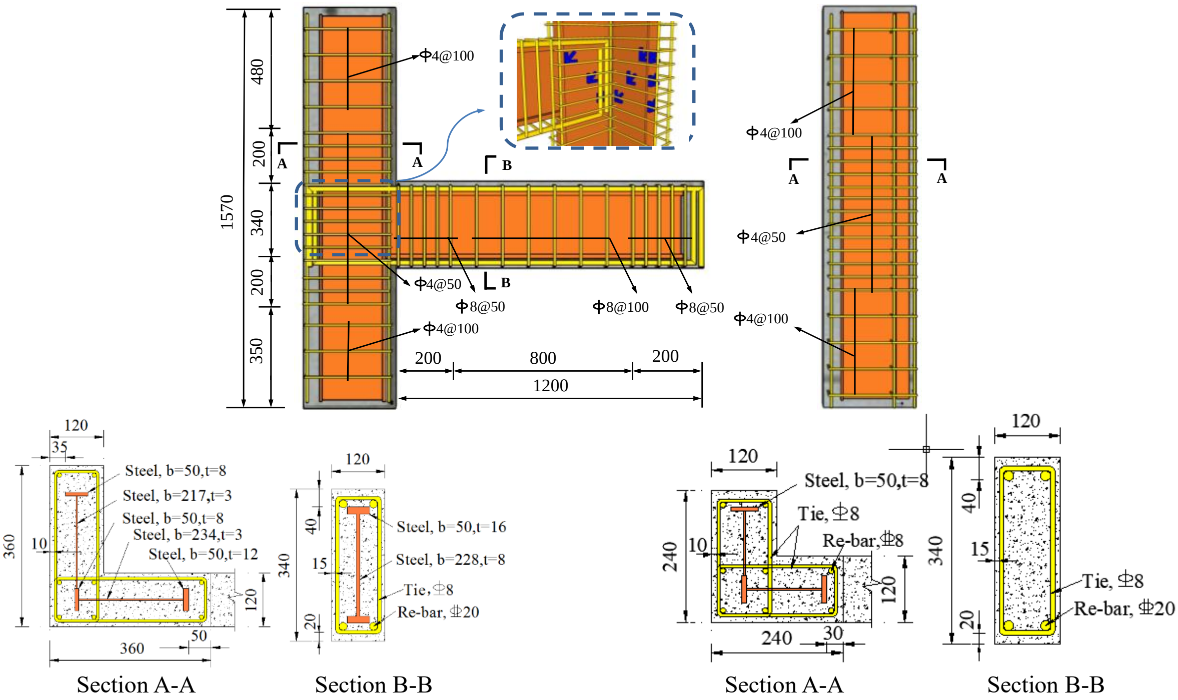

Fig. 1 Details of specimens PLJ3 and PLJ4

types of composite column hold favorable seismic ability.

For the frame structure, the column-beam joint, especially the corner one, has been regarded as the critical member, which prior to failure than others, consequently performing as weak links in the structure. Most of the early research focused on the reinforced concrete steel (RCS) frame system composed of steel beams and RC columns. Different design parameters about the connections have been investigated to develop a comprehensive understanding of failure mode and force transfer mechanisms (Pantazopoulou and Bonacci 1994, Hakuto *et al.* 2000, Braga *et al.* 2009). Owing to the advantages of the SRC and CFT column, the composite frame including steel beam and SRC or CFT column showed better performance during an earthquake attack and had been popular in the US, China, and Japan. Wakabayashi (Wakabayashi and Minami 1980) initially tested 12 SRC column-beam joints in Japan. Chou and Uang (2007) examine the hysteric behavior of two exterior steel beam-SRC column joints and found that the jacket plates contributed to the increase of the shear capacity. Pan *et al.* (2014) tested four novel ring-beam connections for SRC column and RC beams under monotonic loading. All the specimens are shown to satisfy the design requirement. Beutel *et al.* (2002) had conducted an experimental investigation into the seismic behavior of 6 CFST column and beam joints. Good ductility and energy dissipation capability were observed. Wang *et al.* (2011) focused on the novel spatial connection and presented an experimental investigation on the seismic behavior of H-beam and circular tubular column connection. Considering the fire and corrosion resistance, the use of the SRC column-RC beam joint is a preferred alteration without the beam interrupted, which provided good integrity, high structural damping, and high seismic capacity for the hybrid structure. For special-shaped column frame structure, due to the irregularity of section, high-performance joints of the SRC special-shaped column and SRC beam are urgently required in the industry. To date, limited research was available on this type of joint, and mainly research focused on the T-shaped column-beam joint. Chen *et al.* (2015) test 3 planar SRC T-shaped column-RC beam and 6 spatial SRC T-shaped column-steel beam under constant axial compression and lateral cyclic load to investigate the effect of the steel configuration forms, and lateral loading angle. The test result demonstrated that I-shaped steel and specimen under 45°loading angle achieve better seismic performance. Furthermore, Chen *et al.* (2015) proposed a new seismic-induced damage assessment for the spatial SRC T-shaped column-steel beams joint. Xiang *et al.* (2017) studied the seismic behaviors of joints between SRC T-shaped column and RC beam under bidirectional cyclic loading experimentally. Their test result indicated that the shear capacity was undertaken by the steel after cracking and the connections show excellent seismic performance.

In this study, aimed to fill the research gap of the L-shaped column-beam joint, experimental work was performed to investigate the hysteresis behavior of the L-shaped SRC column-RC beam joints. Due to the randomness of the earthquake, these joints were separated into planar and spatial joints two groups to investigate the effects of steel configuration form, axial compressive ratio, and loading angle. Besides, owing to the contribution of the cast-in-place slab, the bending strength of the joint can be significantly increased and the failure mode turns out to be the column-end failure (Prota *et al.* 2004, Ghobarah *et al.* 2006, Park *et al.* 2012). Especially in the Wenchuan

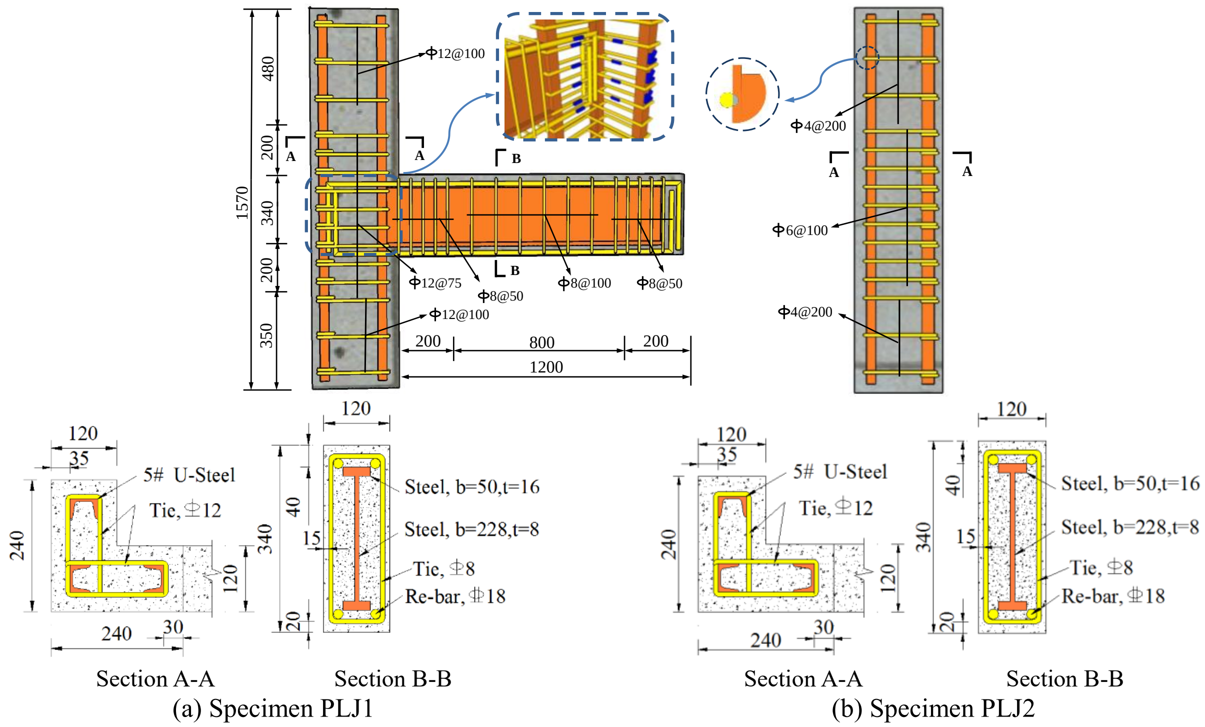

Fig. 2 Details of specimens PLJ1and PLJ2

Table 1 Main design parameters of SRC special-shaped column frame joints with L-shaped cross-section

Specimen label	Steel form	Load angle α/°	Axial load ratio n	Column aspect ratio R	Steel ratio	Reinforcement ratio	f_{cu}/Mpa
PLJ1	U- shaped steel truss	0	0.16	2.0	5.74	0	43.67
PLJ2	U- shaped steel truss	0	0.32	3.0	4.00	0	43.67
PLJ3	Solid-web	0	0.16	3.0	3.81	0.31	43.67
PLJ4	Solid-web	0	0.32	2.0	4.41	0.52	43.67
SJL1	Solid-web	45	0.20	3.0	3.56	0.87	30.63
SJL2	Solid-web	30	0.20	3.0	3.56	0.87	30.63
SJL3	T- shaped steel truss	45	0.20	3.0	3.66	0.87	30.63
SJL4	T- shaped steel truss	45	0.30	3.0	3.66	0.87	30.63
SJL5	U- shaped steel truss	45	0.20	3.0	4.35	0	30.63
SJL6	Reinforcement cage	45	0.20	3.0	0	1.05	30.63
SJL7	Reinforcement cage	45	0.20	3.0	0	1.05	30.63

earthquake in China, because of the RC slab the joint turned out to exhibit the strong beam-weak column behavior (Wang 2008). Hence, the joints with and without slab were carried out to investigate the structural performance. The cyclic characteristics of the L-shaped SRC column-RC beam joints were presented and discussed in terms of failure modes, hysteresis loops, strength, deformation, ductility, stiffness degradation, story drift ratio, and energy dissipation. Furthermore, the design formula of the connections was developed to predict the shear resistance.

2. Experimental programs

2.1 Planar connection specimens detail

The first group of specimens designed to simulate planar connections with SRC L–shaped column and SRC or RC beam. With the scale of 1:2 to the actual structure, four specimens (labeled as PL1, PL2, PL3, and PL4) with several parameters described as cross-sectional steel form, axial compressive ratio, and aspect ratio of the column climb (aspect ratio, the ratio of the depth along the longer side direction to the width along the shorter side direction) were constructed and tested. Specimen subassembly cross-

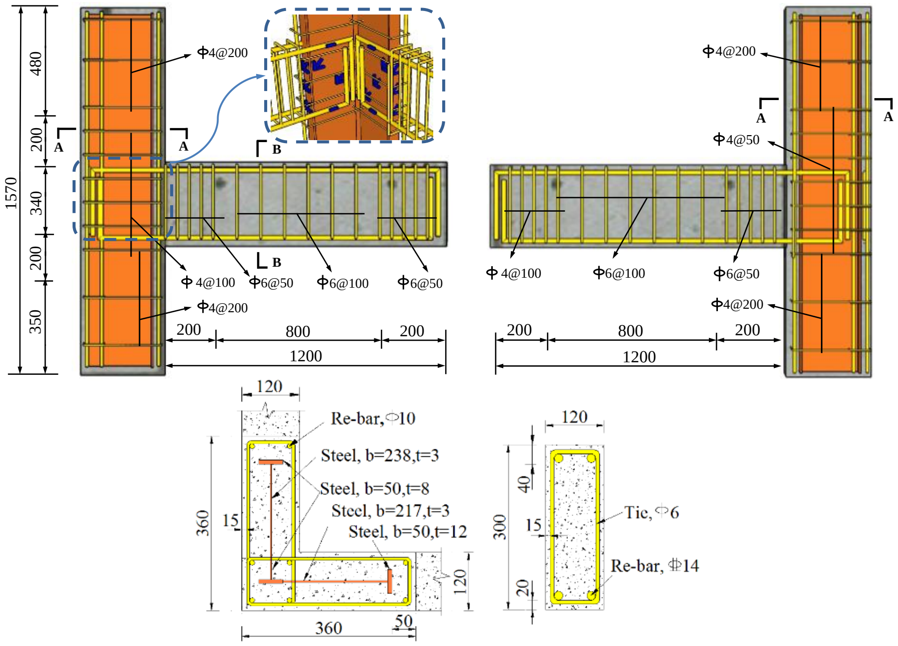

(a) Specimen SLJ1 and SLJ2

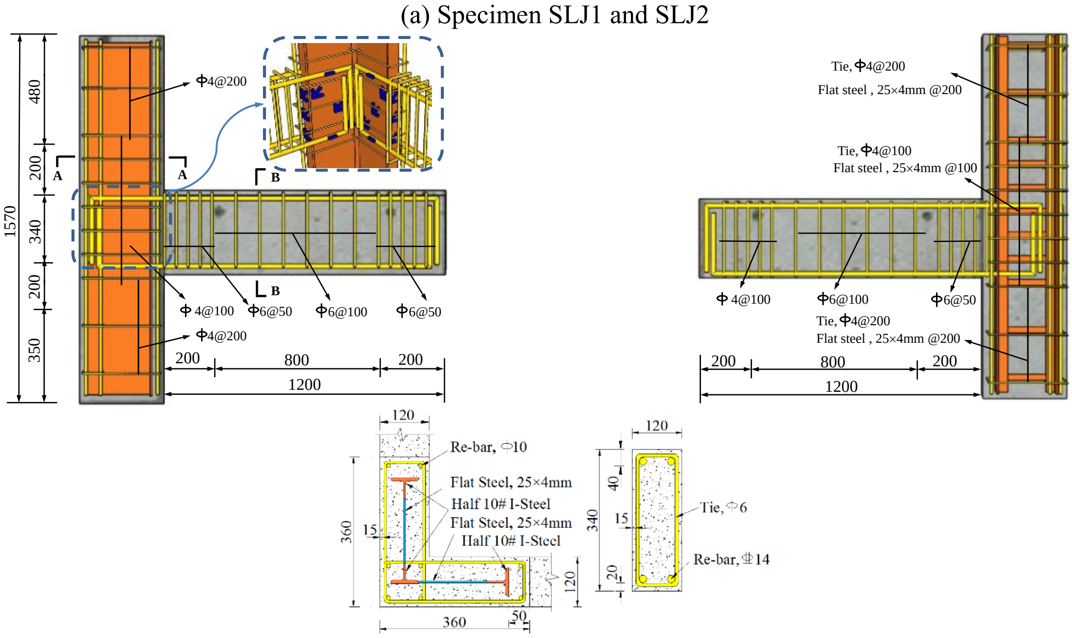

(b) Specimen SLJ3 and SLJ4

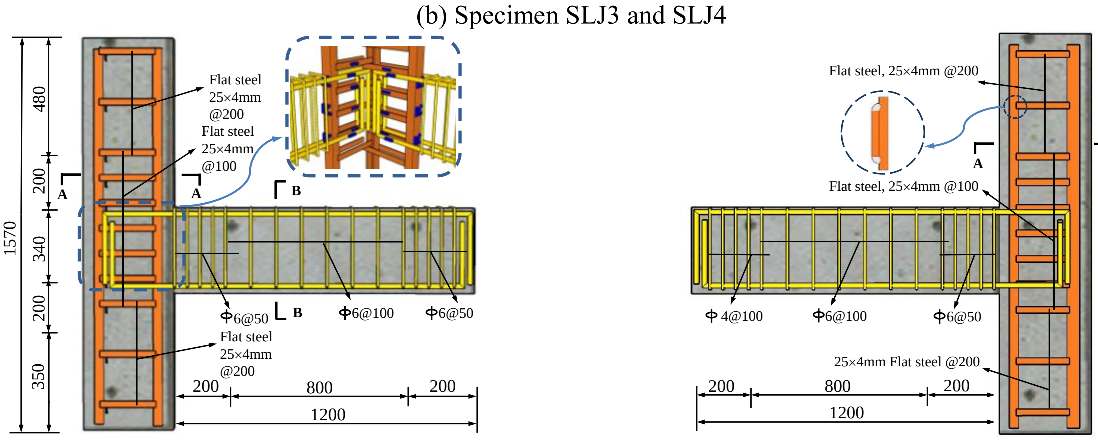

Continued-

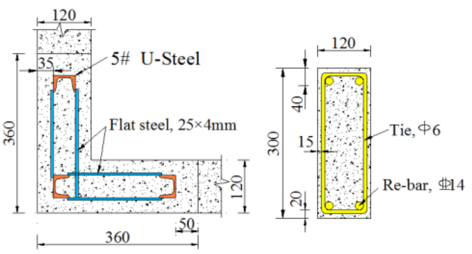

(c) Specimen SLJ5

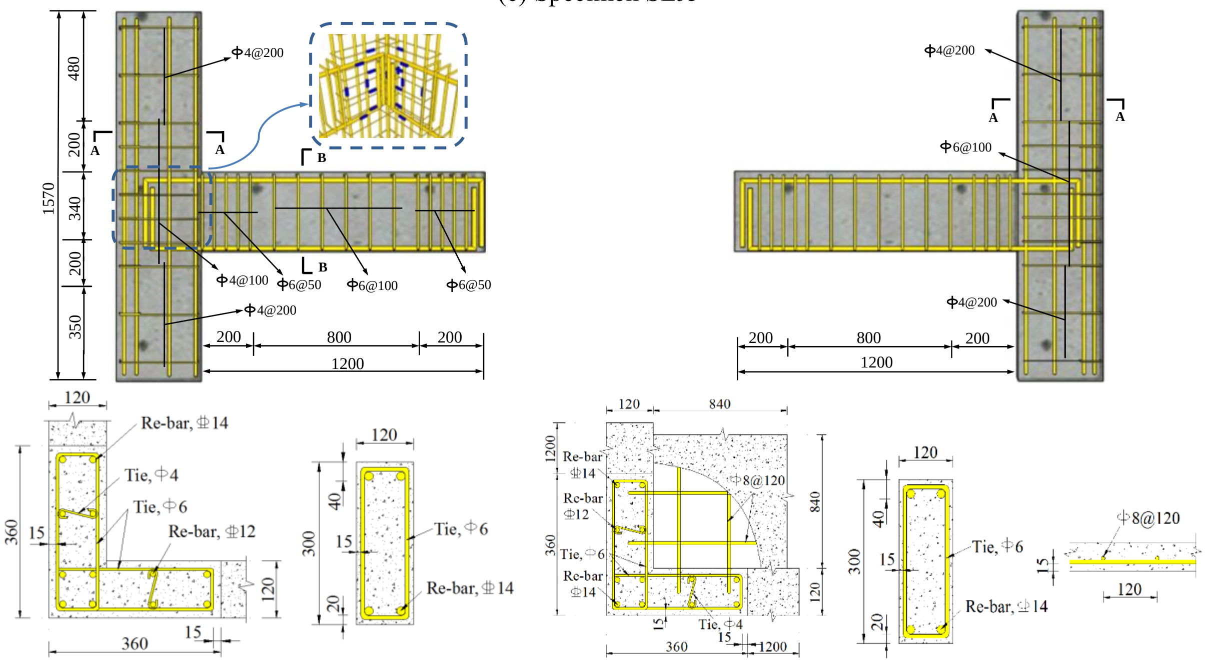

(d) Specimen SLJ6

(e) Specimen SLJ7

Fig. 3 Details of specimens SLJ1, SLJ2, SLJ3, SLJ4, SLJ5, SLJ6 and SLJ7

section dimensions and reinforcing detailing are shown in Figs. 1 and 2. The specimens included two joints consisted of SRC beam and SRC column formed with steel channel (PJ1 and PJ2), one joint (PJ3) consisted of SRC beam and SRC column formed with solid-web steel, one joint (PJ4) consisted of RC beam and SRC column formed with solid-web steel. The solid-web steel was weld by three steel plates, while the three U-steel channels were integrated with transverse reinforcement by welding. The axial compressive ratios of the planar specimens are summarized in Table 1. The column segment of the joints including two different cross-sections was intended to provide two aspect ratios of 0.16 and 0.32: PL1 and PL4 were 0.16, while PL2 and PL3 were 0.32. As depicted in Figs. 1 and 2, the net height of the assumed point of contra flexural between the upper and lower column was 1637.5 mm, while the length from the assumed point of the contra flexural at the midspan beam to the surface of the column limb was designed with 1100 mm. Based on the strong column-weak beam design concept, the critical region of transverse reinforcement with the spacing of 75 mm extended to 200 mm above and below the interface of the column and the joint. To avoid the damage of the beam in the supporting end, transverse reinforcements were at a closer spacing of 50 mm extended to 200 mm from the beam-joint interface.

2.2 Space joints specimens detail

The second group of specimens represents 3D connections simulating corner columns of the intermediate layer. Five spatial beam-column joints (labeled as SLJ1, SLJ2, SLJ3, SLJ4, and SLJ5) consisted of SRC L-shaped column and two RC half-beam in the orthogonal direction were tested to study the effect of four design parameters described as steel configuration type, the axial compression ratio, and the loading angle. In addition, the effects of the slab and profile steel in the column were investigated by the two comparative specimens (labeled as SLJ6, SLJ7) consisted of RC L-shaped column and RC beam, especially the SLJ7 with a slab. The column segments of SLJ1 and SLJ2 include solid-web steel welded by four steel plates and the SLJ3 and SLJ4 consist of T-shaped lattice skeleton weld by half I-steel and flat steel. The SLJ5 contained a U-shaped steel truss consisted of four steel channels welded by the reinforced bars. The axial compressive ratios of the spatial specimens are summarized in Table 1. All the spatial specimens were under 45° loading angle except that the SLJ3 was under 30° loading angle. All the specimens were designed with half scale. The net height between the assumed points of contraflexure in the upper and lower column was 1600 mm, while the length from the assumed

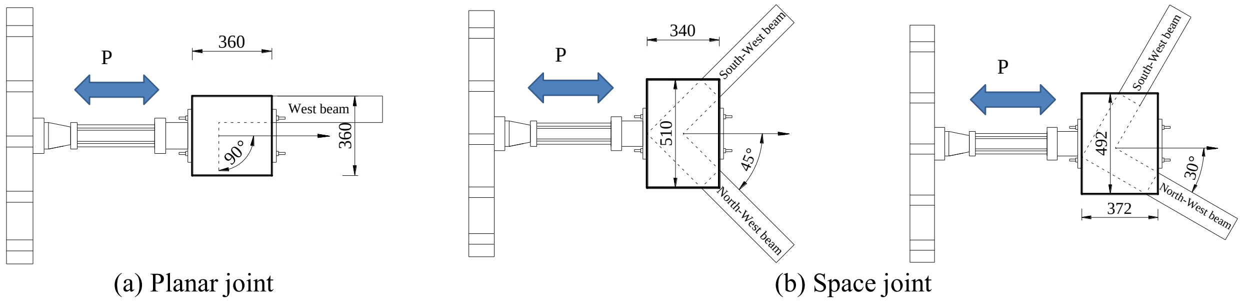

Fig. 4 Loading angles of joints

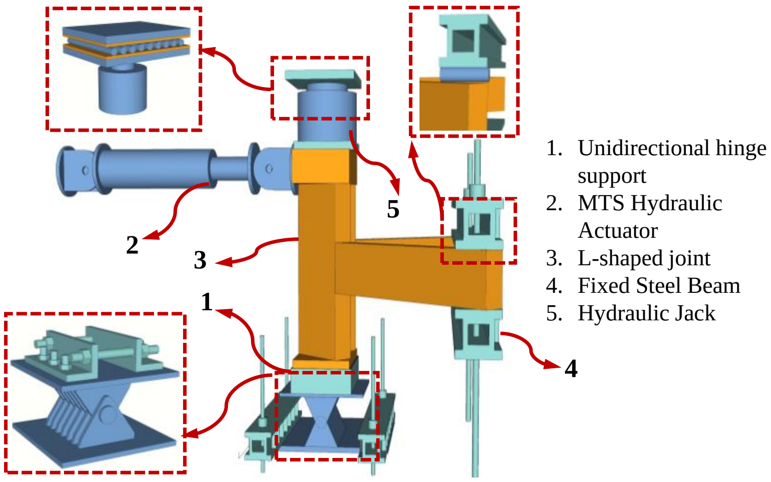

Fig. 5 Test set-up

point of contraflexure in the beam to the surface of the connection was designed with 1100 mm. Fig. 3 shows the dimensions of the specimens and reinforcement details. The main design parameters of the SRC L-shaped column and RC beam joints are presented in Table 1. The material properties of concrete, steel, and bars are summarized in Table 2.

2.3 Experiment Setup, Instrumentation, and Testing Procedures

All the specimens were subjected to quasi-static reversed cyclic loading applied at the top of the column. A constant vertical load was applied on the top of the column through the hydraulic jack and the hydraulic actuator was installed across the reaction wall on the top of the column to provide the horizontal cyclic load. To accomplish the spatial loading on the joint, a special test setup and devices were independently designed by our group for 3D joint specimens meaning that the angle between the lateral load direction and engineering axis (defined as load angel) could be altered as wished. The column segment was pinned supported at the bottom using the self-designed device of unidirectional hinge support. The end of the column was attached with the steel jacket to make sure the column was fixed on the upper plate of the unidirectional hinge support. At the top of the column, a hydraulic jacket with the steel rollers bearing was applied to offer the axial compression load. The steel rollers bearing with a polytetrafluoroethylene plate was used to reduce the friction between the hydraulic jack and the top rigid girder, allowing the specimen to move smoothly when the specimens were subjected to combined vertical compression and horizontal cyclic load. The two orthogonal beams were defined as the south-west (SW) beam and the north-west (NW) beam according to the direction they pointed. The beams were pin-supported at the end by the steel roller. These rollers were welded at the fixed steel beam to restrain vertical direction displacement whereas their rotations were allowed, which earthquake action in any direction could be simulated. A schematic of the loading apparatus is shown in Fig. 5. The load angle of the L-shaped SRC column-concrete beam joint specimen was depicted in Fig. 4.

A force and displacement-controlled mode was applied in the test. At first, all the specimens were loaded in the force-controlled mode with uniform 10 kN increment in planar joints and 5kN increment in space joints until the initial yielding of the steel, respectively. Every load cycle was repeated once. After the steel yielding, the displacement-controlled sequence consisted of three repeated cycles with a progressively increasing displacement amplitude (by 5 mm) in each direction. Until the specimen horizontal carrying capacity decreased to 85% of the peak bearing capacity or the specimen loaded to failure, the loading procedure got terminated.

Table 2 Material test results of steels

Specimen	Tested items	Yield strength	Ultimate strength	Elastic modulus
Planar joint	Φ 4	425	444	1.965×105
	Φ 6	551	674	1.944×105
	Φ 8	441	543	1.921×105
	Φ 12	295	440	1.970×105
	Φ18	453	501	2.010×105
	Φ20	432	487	2.050×105
	5# U-steel	363	409	2.090×105
	3 mm plate	295	385	1.950×105
	8 mm plate	363	503	1.946×105
	12 mm plate	305	367	1.970×105
	16 mm plate	320	365	1.980×105
Space joint	Φ 4	425	444	1.970×105
	Φ 6	437	561	1.810×105
	Φ 8	321	436	1.830×105
	Φ 10	321	436	1.800×105
	Φ12	421	579	1.780×105
	Φ14	412	580	1.950×105
	3 mm plate	318	447	1.760×105
	25×4 mm Flat steel	351	470	1.950×105
	5# U-steel	460	610	1.9920×105
	10# I-steel	308	415	1.896×105
Concrete strength f_c'	Compressive strength:22.8 Mpa, Tensile strength: 2.06 Mpa, Modulus of elasticity: 29791 Mpa			

During the test, the following is monitored and recorded:(1) axial force and horizontal loads on the top of the column, (2) lateral drifts on the top (3) strains of reinforcing steel bars and shaped steel, (4) joint shear strains of concrete. Axial force and horizontal loads on the top of the column were measured by the force cells. The drift of the column top along with the lateral load direction was monitored by the displacement sensor. The strain was recorded by TDS-602 data collection instrument gauges at the predetermined positions on joint core steel and reinforcing skeleton cage including flange and web steel in solid-web steel specimen, flange, and horizontal web member in hollow steel specimen, longitudinal and transverse reinforcements, and steel and reinforcement in the beam. Three directional strain gauges (rosette strain gauges) are stuck to the joint panel zone to calculated corresponding strains. The layout of the instrument at the joint zone was shown schematically in Figs. 1-3.

3. Test result and evaluation of structural performance

In this paper, all the specimens were divided into two groups according to the steel configuration type in the column segment. One group of connections consist of the SRC column with the solid-web steel was determined as the solid-web group. And the rest of the specimens were determined as hollow-web group including steel channel truss, T-shaped steel truss, and reinforcement cage.

3.1 Failure mode and process

3.1.1 Failure mode of planar connection

The failure process of the planar connection was generally similar to each other. Thus, a representative specimen of PLJ1 was selected. During the load controlled procedure, at the 20 kN of the lateral load, a few flexural cracks were initiated at the beam. At the 30 kN of lateral load, as the flexural crack propagating in a stable manner, many fine diagonal cracks were observed on both sides of column limb at the beam joint. at the 40kN of lateral load, new diagonal cracks increased on the interface between the column limb and the joint zone, and the cracks propagated to the old diagonal crack. A few horizontal cracks occurred on the exterior face of the column limb that is orthogonal to the beam. At the 50 kN, crosswise cracks propagated toward the column limb at the beam connection, and vertical cracks were detected on the corner of the column. During the displacement controlled procedure, in the first displacement amplitude cycle, the flexural-shear crack grew widened and deep in the joint zone, and cover concrete was split into rhombus-shaped pieces. In the second cycle, the flexural-shear crack propagated in a vertically upward and

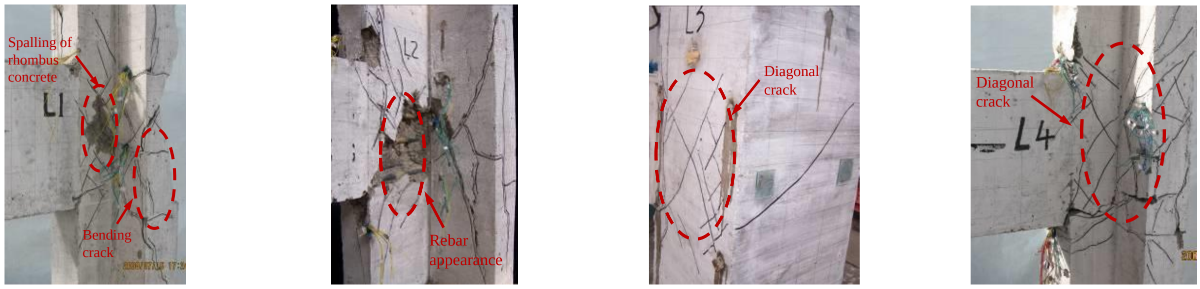

(a) Specimen PLJ1 (b) Specimen PLJ2 (c) Specimen PLJ3 (d) Specimen PLJ4

Fig. 6 Damage mode of the planar joint at the end of the test

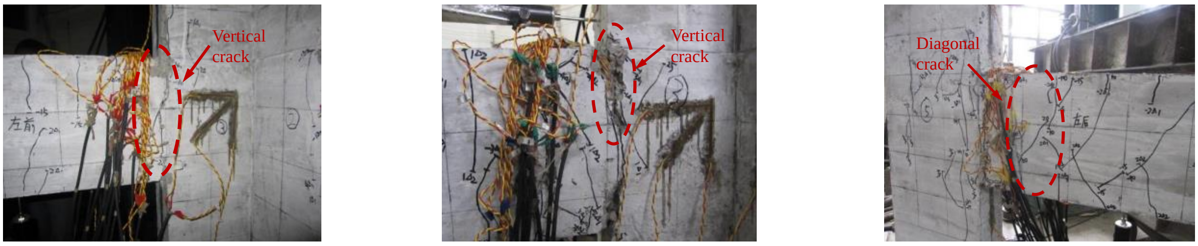

(a) Specimen SLJ1 (b) Specimen SLJ2 (c) Specimen SLJ3

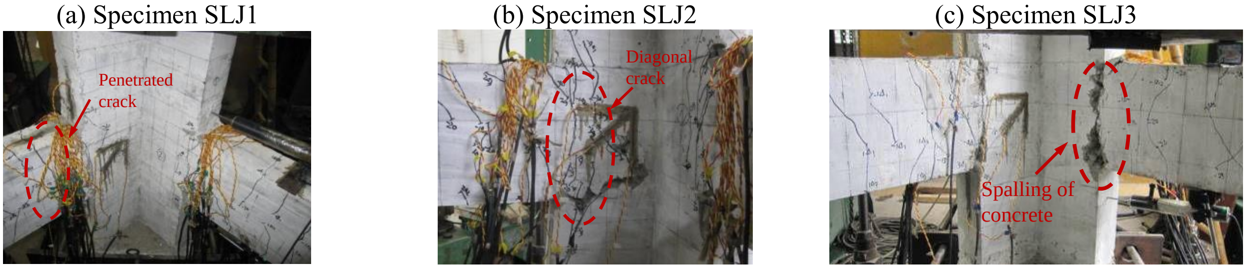

(d) Specimen SLJ4 (e) Specimen SLJ5 (f) Specimen SLJ6

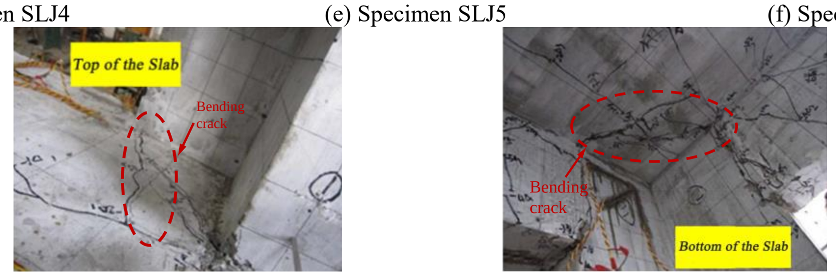

(g) Specimen SLJ7

Fig. 7 Damage mode of the space joint at the end of the test

downward direction to the top and bottom of the beam, respectively, while concrete encasement began to spall. in the third cycle, the rhombus-shaped cover concrete in the joint core crush to spall and steel plate was exposed. Thereafter, when the specimen entered the failure stage, the concrete on the top and bottom column limb close to the beam-column interface was crushed, and longitudinal bars were exposed. The specimen exhibited shear failure in the joint panel zone. All failure modes of the specimens were illustrated in Fig. 6.

3.1.2 Failure mode of spatial joint

Excerpt for the SLJ5, the failure process of the spatial joints were generally similar to each other. Thus, The SLJ3 was selected as a representative. During the load-controlled procedure, at the 10 kN of the lateral load, a vertical crack was initiated on the NW beam within the distance of 100 mm from the joint face connected to the beam. At the 15 kN of the lateral load, several vertical cracks were observed ranged from 200 mm to 300 mm apart from the tip of both the beams and original cracks keep propagating toward the bottom of the beam. At the 20 kN, the flexural cracks increased on the beam. During the displacement-controlled procedure, in the first displacement amplitude cycle new vertical cracks were observed on the beam at a distance equal to 600 mm from the beam-column interface, while the flexural shear crack occurred on the beam 600 mm apart from the column connection. In the second cycle, from 300 mm to the interface of the NW beam and column limb vertical cracks were observed intersected the beam. Few cracks occurred on the column-beam interface. In the third cycle, vertical bond cracks occurred on the concrete encasement where the steel was seated in the column limb.

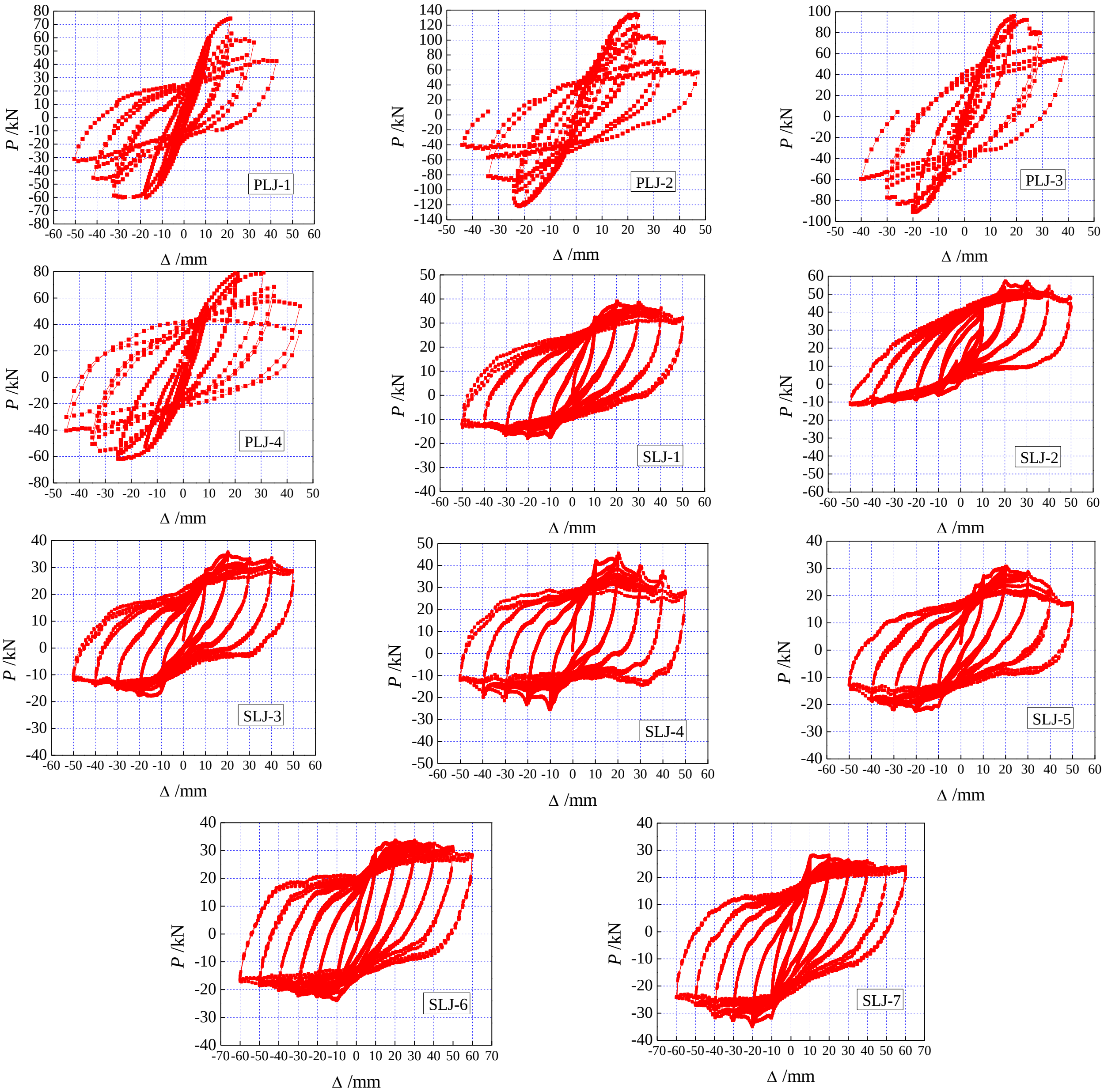

Fig. 8 Lateral load-displacement relationships of the specimens

The cracks gradually propagated and grew widened, the concrete was locally delaminated at the beam tip. In the fourth cycle, the diagonal cracks intersected on the transition between the column and beam. The cover concrete was split into rhombus pieces. With the crushing zone of the beam expanding, the plastic hinges were formed. Henceforth, until the specimen crushed there was no new crack appeared. In the final failure stage, the flexural failure in the beam tip was observed in these specimens.

As specimen SLJ5, during the initial loading stage, bending cracks were concentrated on the tip of the beam. With the increase of the load, diagonal cracks were detected in the joint panel connecting the beam. After that, the two kinds of cracks propagated stably in the beam and joint zone. The flexural-shear failure was dominated at the end of the test. Furthermore, for the specimens SJL7 with a slab, the bending failure was noticed at the slab and the plastic hinge developed at the beams ends. The distribution of the cracks on the top and bottom of the slab were shown in Fig. 7. All the failure modes of the specimens were also shown in Fig. 7.

3.2 Lateral load–displacement relationship

The hysteretic responses of load-displacement on the column tip for the specimens are shown in Fig. 8. The skeleton curves of these specimens were depicted in Fig. 9. The following observations can be summarized from these envelopes:

(1) For the specimens without a slab, the asymmetry of the hysteretic loops, in which the peak strength in the positive direction is greater than in the negative direction, was ascribed to the failure mode of specimens. In the positive loading direction, the specimens were dominated

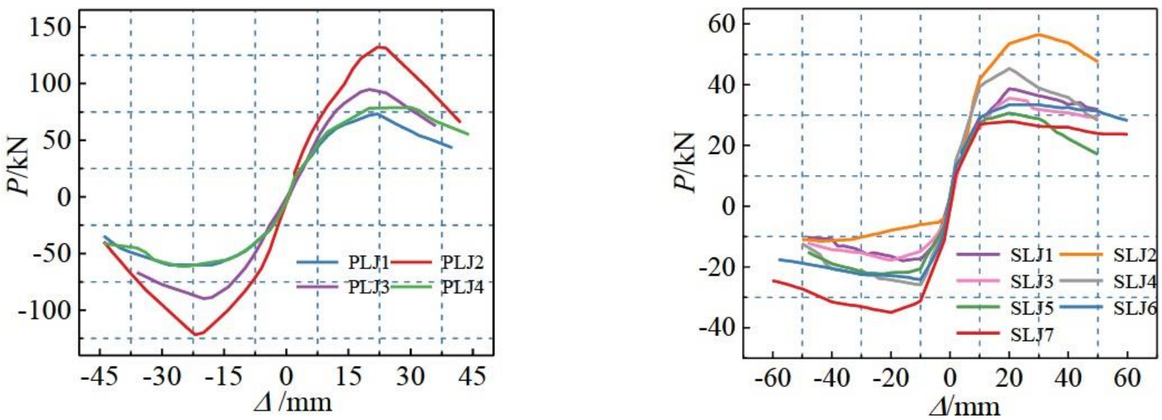

(a) planar joint (b) spatial joint

Fig. 9 Skeleton curves

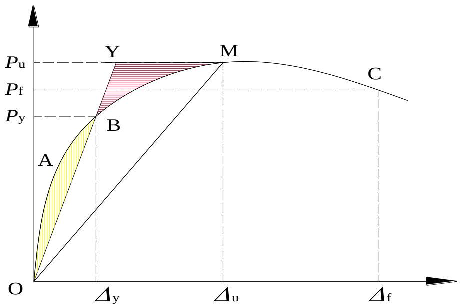

Fig. 10 Characteristic points of skeleton curve for frames

by the flexural cracks on the outer face of the column. In addition, the face connected to the beam developed fewer cracks attributed to the constraint by the beam, which is effective in resisting the shear. In the negative loading direction, due to the drag force by the beam, the joint panel got weaken and exhibited heavy shear damage. Meanwhile, the bonding failure at the interface between the column and beam is more serious. For the specimens with a slab, the effective confinement of the slab contributed to the joint panel resulted in a higher capacity in the negative direction than the contrary direction, which the final failure occurred in the junction between the slab and the beam. Besides, no severe damage appeared in the joint panel.

(2) The hysteretic loops of the solid-web group were plumper than that of the hollow-web group.

(3) In the same condition, the degree of pinching in the loops of the specimen with 0.3 of the axial compressive ratio was relatively high compared with the specimens with the ratio of 0.4. This is attributed to the low ductility caused by the high axial compressive ratio, which reduced the energy dissipation. The specimen with a high axial compressive ratio shows a high degree of pinching in the loops.

(4) The slope of the envelope after the peak load was steeper, while the response of the spatial joint dropped gently. It was noted that the shear capacity of the spatial joint is lower in comparison to the planar joint after the

(5) specimen entering the negative stiffness. It was indicated that the failure occurred on the beam-end has better ductility than the shear failure of the joint panel.

3.3 Load-carrying capacity

The characteristic points (namely, the yielding load P_y and yielding displacement Δ_y, peak load P_u and peak displacement Δ_u, ultimate load P_f and ultimate displacement Δ_f) of the specimens, which were defined on the skeleton curve, are listed in Table 3. The yield load P_y is related to the yield displacement Δ_y which is defined based on criteria for equivalent elastic-plastic energy absorption. The peak displacement Δ_u refers to the peak load P_u which is the maximum lateral load. The failure load P_f was defined as the post-peak displacement corresponding to 85% of the peak strength. The criteria of equivalent elastic-plastic energy absorption is shown in Fig. 10.

The normalized average joint capacity, ω, is expressed as $\omega = P_u \times 10^3/(f_c\ b_c\ h_0)$. Where, P_u = the peak load in kN; b_c = width of the column climb in mm; h_0 = effective depth of the column climb in mm, $h_0 = h - a_c$, h = total height of the cross-section in one direction. A_c = thickness of the cover concrete from longitudinal reinforcement or the steel along with the direction of h_0 in mm. For the planar joint, the direction of h_0 was defined as the direction parallel to the shear. As a spatial joint, h_0 was corresponding to the maximum of the column limb length. The calculated result is presented in Table 3.

Table 3 Feature point values of test results

]	P_y /kN		Δ_y /mm		P_u /kN		Δ_u /mm		P_f/kN		Δ_f/mm		$\omega = P_u \times 10^3/(f_c b_c h_0)$		
	+	-	+	-	+	-	+	-	+	-	+	-	+	-	average
PLJ1	63.1	47.0	12.4	9.7	74.4	60.1	21.4	28.2	63.2	51.1	27.6	37.2	0.089	0.072	0.080
PLJ2	94.4	84.0	13.0	10.2	135.0	122.0	23.0	22.0	114.8	103.7	30.0	29.4	0.109	0.099	0.104
PLJ3	84.8	81.4	14.1	14.6	95.7	91.0	19.0	19.0	81.4	77.3	28.3	29.8	0.069	0.065	0.067
PLJ4	63.0	45.1	12.5	9.1	79.2	61.7	31.0	25.0	67.3	52.4	35.7	33.0	0.086	0.067	0.077
SLJ1	31.1	13.4	13.1	7.0	36.5	17.4	29.7	9.9	31.0	14.7	50.0	31.8	0.044	0.021	0.032
SLJ2	49.9	5.5	16.7	8.2	56.8	11.9	30.0	39.9	48.3	10.1	49.1	50.4	0.068	0.014	0.041
SLJ3	29.5	12.7	11.9	7.9	35.9	17.7	20.3	20.0	30.5	15.1	44.2	32.1	0.043	0.021	0.032
SLJ4	39.6	18.6	9.8	7.0	45.7	25.6	20.2	10.1	38.8	21.8	30.8	29.0	0.055	0.031	0.043
SLJ5	25.9	17.9	9.6	8.7	30.9	22.5	20.1	20.0	26.2	19.2	34.0	38.4	0.041	0.030	0.036
SLJ6	25.2	18.2	7.6	6.5	33.5	23.9	20.0	10.0	28.5	20.3	60.1	40.5	0.040	0.029	0.035
SLJ7	21.5	27.7	7.3	8.7	28.2	34.9	20.0	20.1	24.0	29.6	49.9	44.0	0.034	0.042	0.038

(1) From Table 3, it is observed that the normalized average capacity of the planar joint is generally half of that for the spatial joint. It is attributed to the singular beam connected to the planar joint, while the spatial joint has two orthogonal beams. The L-shaped column climb of the planar joint in the orthogonal direction to the singular beam act as a flange which could provide the confinement effect to the joint panel. As a result, it improved the joint performance in the deformation and strength. Whereas, due to the two orthogonal beams, the spatial joint subjected to the collective force from two orthogonal beams under cyclic load result in the spalling of concrete in the core area prematurely. And it turns out to be low strength for space joint.

(2) It was observed that the increase of normalized average capacity ω for SJL6 is 8.57% compared to the specimen SLJ6 without a slab. It is indicated that the shear capacity of the spatial joint increase with the existence of the slab. The specimen of SLJ1 under loading angle 45° only reached 78.05% of the normalized average capacity ω for the specimen SLJ2 under loading angle 30°. It is revealed that the specimen under 45° has a lower shear capacity compared to the loading angle of 30°, which is in accordance with the formula proposed in the following section.

(3) With the increase of axial compression ratio, the normalized average capacity ω of planar joint with steel channel truss, planar joint with solid-web, and spatial joint with T-shaped truss improved by 30.0%, 15.9%, and 34.3%, respectively. It is indicated that the axial compression ratio has a significant improvement on the shear strength for both planar and space joint. This is because the performance of concrete improved in the high triaxial compression.

(4) To evaluate the contribution of the steel in the column, the specimens (SLJ1, SLJ3, and SLJ5) with the SRC column were compared to the RC specimen SLJ6. It was found that in the positive direction the normalized capacity of specimens SLJ1, SLJ3, and SLJ5 were relatively higher than the specimen SLJ6, while it is opposite in the negative direction. The reasons were as follows: ① The Bauschinger effect of the steel was enhanced with the increase of the ratio of the steel section to the column cross-section, which resulted in the reduction of the capacity in the negative direction. ② During the loading procedure the steel did not significantly affect the joint behavior because the beam failed before the joint.

3.4 Displacement ductility factor

Base on the standard of GB 50011-2010 (China 2010) code for seismic design of buildings, displacement ductility factor μ can be calculated as follows

$$\mu = \Delta_f / \Delta_y \tag{1}$$

Where, Δ_f = the ultimate displacement in mm; Δ_y= the yielding displacement in mm. The calculated values μ were list in Table 4.

As described in Table 4, the values μ for the planar joints were lower than the spatial joint. This is because the orthogonal beams of the spatial joints provided stronger confinement to the core zone of joints compared to the planar joints. It is indicated that the spatial joint has a better performance in displacement ductility compared to the planar joint, which is agreed with the bending failure in the beam tip for the spatial joint and shear failure in the joint panel for the planar joint.

3.5 Story drift ratio

The story drift ratio θ is an important index to evaluate the anti-collapse strength, and its calculation is as follows

$$\theta = \frac{\Delta}{L_1 + L_2} \tag{2}$$

Where, Δ = the horizontal displacement at the top of the column; L_1 and L_2 = the distance from the upper or lower contraflexural point to the center of the joint zone, respectively.

Table 4 Displacement ductility factors, equivalent viscous damping coefficients, and layer displacement angles of specimens

Specimen label		PLJ1	PLJ2	PLJ3	PLJ4	SLJ1	SLJ2	SLJ3	SLJ4	SLJ5	SLJ6	SLJ7
h_e in the failure cycle		0.204	0.252	0.254	0.241	0.442	0.368	0.419	0.577	0.538	0.438	0.420
μ	+	2.22	2.30	2.01	2.85	3.83	2.94	3.73	3.14	3.55	7.91	6.80
	-	3.84	2.87	2.04	3.67	4.52	6.12	4.08	4.13	4.42	6.19	5.08
	average	3.03	2.59	2.03	3.26	4.18	4.53	3.91	3.64	3.99	7.05	5.94
θ_y	+	1/125	1/125	1/111	1/125	1/122	1/96	1/134	1/163	1/167	1/211	1/219
	-	1/167	1/167	1/111	1/167	1/228	1/195	1/203	1/229	1/184	1/246	1/184
θ_f	+	1/58	1/55	1/58	1/45	1/32	1/33	1/36	1/52	1/47	1/27	1/32
	-	1/43	1/55	1/55	1/50	1/50	1/32	1/50	1/55	1/42	1/40	1/36

According to GB 50011-2010 (China 2010), the limit of the elastic story drift ratio θ_e and the limit of elastoplastic story drift ratio θ_p for the RC frame structure are 1/550 and 1/50, respectively. Table 4 shows the story drift ratios of all specimens.

(1) When the specimen reached yield, the story drift ratio of the planar joint θ_y = (3.29~495) θ_e. The story drift ratio of the specimen SLJ2 under load angle 30° is θ_y = 2.87θ_e in the negative direction and θ_y = 5.73θe in the positive direction. The story drift ratio of the SRC spatial joints under the load angle 45° is θ_y = (2.40~5.73)θ_e. The story drift ratio of the RC spatial joint is θ_y = (2.24~2.99) θ_e. Thus, the elastic story drift ratio of L-shaped column-beam joints meets the requirement of the code. In addition, the elastic deformation capacity of SRC column-concrete beam joints is obviously better than RC joints.

(2) When the specimen failed, the average story drift ratio θ_f of the planar joints, SRC space joints and RC space joints are 1/52, 1/36, and 1/33, respectively. Hence, the story deformation capacity of the space joints meets the requirement, and its anti-collapse ability is better than the planar one. This is because the spatial joints have more constraints from the beams, which make it to be statically indeterminate structures.

(3) With the increase of axial compressive ratio, the story drift ratio decreased. Compared with PLJ1 with n=0.16, the story drift ratio of PLJ2 with n=0.32 decreased by 11.3%.

3.6 Hysteretic energy dissipation

In order to evaluate the seismic performance of the specimens, the hysteretic energy dissipation was considered in terms of equivalent viscous damping factor h_e, which is shown in Fig. 11. The h_e can be calculated as follows

$$h_e = \frac{1}{2\pi}\frac{S_{(ABC+CDA)}}{S_{(\Delta OBE+\Delta ODF)}} \tag{3}$$

Where, $S_{(ABC+CDA)}$ = the area enclosed by a complete load cycle; $S_{(\Delta OBE+\Delta ODF)}$ = idealized energy dissipation assuming elastoplastic behavior.

Table 4 shown the equivalent viscous damping factor of all the specimens as they failed. As shown in Table 4, it is evident that h_e for planar joints were lower than those for space joints owing to the more beams that space joint connected. The is because the severe damage could be observed at the junction between the column climb and the beam owing to more beams connected to the joint, indicating more energy dissipated under the cyclic loading. The specimen with the loading angle of 45° exhibits a better energy dissipation capacity. A reduction of 16.7% in energy dissipation was observed for the specimen with the loading angle of 30°, compared to the loading angle of 45°.

3.7 Stiffness degradation

Secant stiffness (K_i) is used to assess the stiffness degradation under different lateral displacement levels

$$K_\Delta = \frac{|P_i^+| + |P_i^-|}{|\Delta_i^+| + |\Delta_i^-|} \tag{4}$$

Where, P_i = the maximum load under the ith loading cycle in kN; Δ_i = the maximum lateral displacement corresponding to the P_i under ith loading cycle in mm.

Fig. 12 showed the relationship between the secant stiffness and normalized yield displacement. In Fig. 12(a), the stiffness of specimens with the column aspect ratio of 3.0 were greater than those with the aspect ratio of 4.0, which is indicated that the secant stiffness is sensitive to the section dimension. Compared to the solid-web specimens, the secant stiffness of the U-steel truss specimens quickly decreased since the high steel ratio of the solid-web specimen resulted in the lighter damage in concrete. In Fig. 12(b), because the cracks were less observed under high axial compression, the initial stiffness increase with the increase of the axial compressive ratio. In the whole loading progress, the secant stiffness of specimen SLJ7 is greater than specimens SLJ6. It is indicated that the contribution of the slab is significant to the stability of the joint zone. In the initial loading stage, the stiffness of the RC column-concrete beam joint was higher in comparison to the SRC joint. Because during that stage the concrete was the main resistance member, the contribution of the steel or

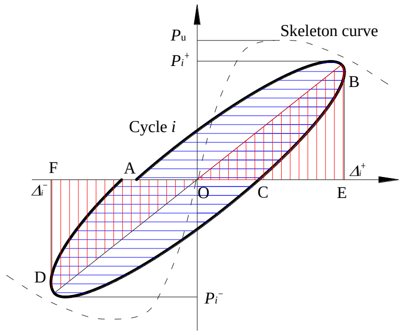

Fig. 11 Energy dissipation

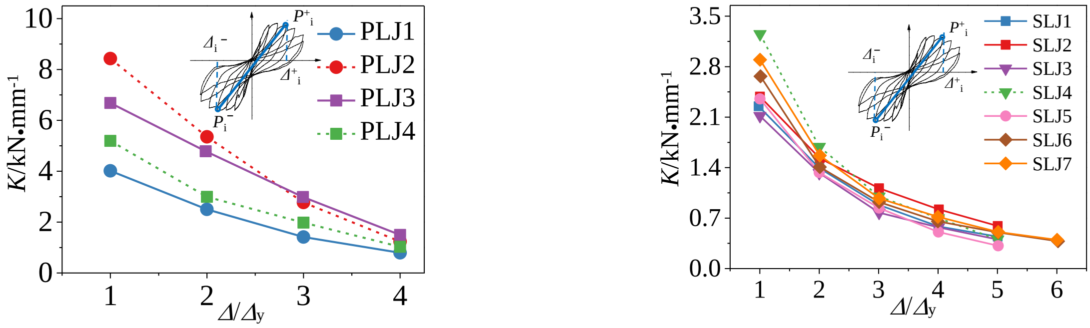

(a) planar joint

(b) Space join

Fig. 12 Degradation of secant stiffness

reinforced bar relatively less than the concrete. In addition, the secant stiffness of solid-web specimens is greater than the hollow-web steel specimens.

4. Shear Capacity of joint

4.1 Shear capacity along the principal axis of the joint

Based on the previous research (Chen and Lin 2009, Montava Belda *et al.* 2019, Xu *et al.* 2020), the superposition method was able to accurately estimate the shear strength of the SRC joint. Namely, the shear strength contributed by steel shape, the transverse reinforcements, and the concrete shear. In this study, the superposition theory and equilibrium plasticity truss model were used to estimate the shear strength of the concrete. Our early work obtained the relationship of the compressive ratio and shear capacity in the method of finite element analysis. According to the finding, the shear strength V_j of the different type joints can be calculated as follow:

1) Solid-web steel L-shaped column-beam planar joint can be calculated as follows

$$V_j = 0.5(0.69 - 0.4n)\eta\xi_f b_j h_c f_c\left(\sqrt{1+\left(\frac{h_b}{h_c}\right)^2} - \frac{h_b}{h_c}\right) + \frac{A_{sv}}{s_{sv}} f_{sv}(h_0 - a_r') + \frac{1}{\sqrt{3}} h_w t_w f_y \quad (5)$$

2) T-shaped truss L-shaped column-beam planar joint can be calculated as follows

$$V_j = 0.5(0.70 - 0.6n)\eta\xi_f b_j h_c f_c\left(\sqrt{1+\left(\frac{h_b}{h_c}\right)^2} - \frac{h_b}{h_c}\right) + \frac{A_{wh}}{S_{wh}} f_{wv}(h_0 - a_r') + \frac{A_{sv}}{S_{sv}} f_{sv}(h_0 - a_r') \quad (6)$$

3) U-steel truss L-shaped column-beam planar joint can be calculated as follows

$$V_j = 0.5(0.80 - 0.8n)\eta\xi_f b_j h_c f_c\left(\sqrt{1+\left(\frac{h_b}{h_c}\right)^2} - \frac{h_b}{h_c}\right) + \frac{A_{wh}}{S_{wh}} f_{wh}(h_0 - a_r') \quad (7)$$

Where n= axial compression ratio; η= width coefficient of concrete diagonal compressive strut referred to the location of the joint in the structure, which was determined as 0.8 in this study owing to the corner joint; ξ_f = coefficient of the flange, which is 1.05 and 1.1 for 120 mm and 240 mm of the extensive length, respectively; b_j= width of the joint core section (b_j=b_b+0.5b_c ,when width of the beam is less than the width of the column climb; otherwise, b_j=b_c); b_c = width of the column climb; h_c = depth of the column climb in the direction of the shear; f_c= concrete prism strength, f_c=0.76f_{cu}; h_b= width of the beam; A_{sv} = the total area of the transverse reinforcement perpendicular to the column climb; S_{sv}= spacing of the transverse reinforcement;

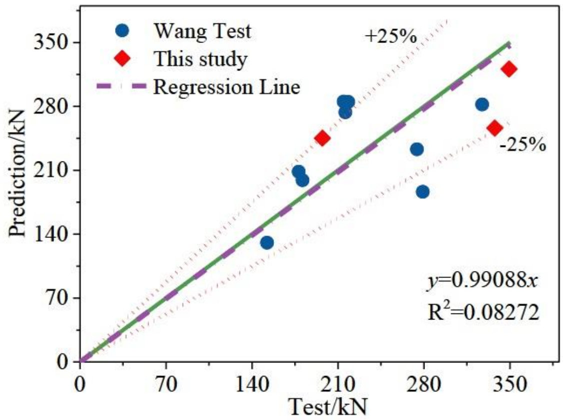

(a) Shear failure mode

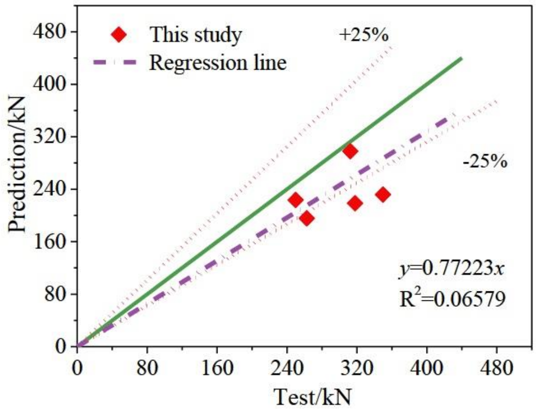

(b) Bending failure mode

Fig. 13 Comparison of the calculated and the experimental strength of the joints

f_{sv} = yield strength of the transverse reinforcement; a_r' = the distance from longitudinal tension reinforcement to the extreme compressive fiber of concrete or the centroidal axis of steel flange; h_w = steel web width; t_w = steel web height; f_y = yield strength of steel web; A_{wh} =the total area of horizontal steel web in hollow-web specimen; S_{wh} = the spacing of the horizontal steel web in hollow-web specimen; f_{wh} = yield strength of the horizontal steel web in hollow-web specimen.

4.2 Shear capacity affecting by load angle

Our group (Wang 2013) obtained the relationship of the shear strength of L-shaped column-beam space joint and planar joint under any angle by regression analysis of the finite element model.

$$V_{j,\alpha} = V_j\sqrt{\cos\alpha + \sin\alpha} \tag{8}$$

4.3 Comparison and analysis of the predicted result and test result

Based on the equilibrium of moments, the formula of shear capacity for the joint along with one principal axis could be expressed as follow

$$V_j = \frac{M_b}{h_{bw}}\left(1 - \frac{h_{bw}}{h-h_b}\right) \tag{9}$$

$$M_b = V_c(h - h_b) \tag{10}$$

Where, $\mathrm{M_b}$ = beam end moment of the joint; $\mathrm{V_c}$ = the lateral load at the top column; $\mathrm{h_{bw}}$ = distance between the centroidal axis of top and the bottom steel flange or center-to-center distance between the compressive and tensive reinforced bars; h = the distance between the upper and the lower counterflexural point of the column.

To assess the applicability of the calculation method mentioned above, 9 extra L-shaped SRC column-steel beam or SRC beam joints (N 2014) which exhibited shear failure in the joint panel was applied for supplementary calculation. All the calculated results are presented in Fig. 13. A regression line was provided to better highlight the accuracy of this method in predicting the strength. For joints with the shear failure mode, the slope of the regression line is 0.99088, which indicating the method agreed well with the test result. The joints with bending failure mode in the beam tip are mainly spatial joint. The slope of its regression line is 0.77223. It is indicated that the method underestimated the strength of the spatial joint, which is in accord with the design concept of the strong joint.

5. Conclusions

Based on the test investigation presented herein, the major findings of the study are summarized as follows:

- The failure mode of the L-shaped SRC column-concrete beam planar joint specimen is mainly the shear failure in the joint panel zone, while the L-shaped reinforced column-reinforced beam space joint specimen is plastic hinge failure in the beam tip. As to the failure model of specimen L-shaped SRC column-concrete beam space joint with the slab, the tip of the beam occurred plastic hinge and the floor slab is bending failure.
- The hysteresis loop of the SRC L-shaped column-RC beam joint specimen is remarkable asymmetry, and the hysteretic curve of solid-web specimens is plumper than that of the hollow-web specimen. It is attributed that the steel in the L-shaped column only enhances the bearing capacity in one direction, while the bearing capacity in the other direction is affected by Bauchenger effect significantly.
- The normalized capacity of the space joint under 30° load angle is greater than that under 45°. The existence of slab has a significant contribution to the improvement of the load capacity and the stability of the stiffness. The high compression ratio contributed to the increase in capacity and initial stiffness of the joint.
- Comparing the planar joint and spatial joint, the relative bearing capacity of the former is higher while the latter has better performance at energy dissipation, displacement ductility, and collapse resistance. In

general, the elastic and elastic-plastic story deformation capacity of L-shaped column frame joints are greater than the code requirement of 1/550 and 1/50.

- In view of the loading angle, the modified calculation method of shear bearing capacity of L-shaped column-beam joint was put forward, and the predicted value of the joint with shear failure mode in the joint core is agreed with the test result. The calculated value of joint occurred beam failure in beam tip is lower than the test value and satisfies the seismic requirements for "strong joints"

Acknowledgments

The research was financially supported by the National Natural Science Foundation of China (N0.50908057 and 51268004), Special Fund Project for "Bagui" Scholars ([2019] No.79), Guangxi Science and Technology Base and Talent Special Project (AD21075031) and Innovation Project of Guangxi Graduate Education (YCBZ2019025, YCBZ2020027).

References

Beutel, J., Thambiratnam, D. and Perera, N. (2002), "Cyclic behaviour of concrete filled steel tubular column to steel beam connections", *Eng. Struct.*, **24**(1), 29-38. https://doi.org/10.1016/S0141-0296(01)00083-9.

Braga, F., Gigliotti, R. and Laterza, M. (2009), "R/C existing structures with smooth reinforcing bars: experimental behaviour of beam-column joints subject to cyclic lateral loads", *Open Constr. Build. Technol. J.*, **3**(1),

Cao, W., Huang, X., Song, W., Tian, B. and Cui, Y. (2005), "Experiment and non-linear element analyses of seismic behavior of short specially shaped columns with crossed reinforcing bars", *Jianzhu Jiegou Xuebao*, **26**(3), 30-37. (in Chinese).

Chen, C.C. and Lin, K.T. (2009), "Behavior and strength of steel reinforced concrete beam–column joints with two-side force inputs", *J. Constr. Steel Res.*, **65**(3), 641-649. https://doi.org/10.1016/j.jcsr.2008.03.010.

Chen, Z., Xu, J., Chen, Y. and Xue, J. (2015), "Seismic behavior of steel reinforced concrete (SRC) T-shaped column-beam planar and 3D hybrid joints under cyclic loads", *Earthq. Struct.*, **8**(3), 555-572. http://dx.doi.org/10.12989/eas.2015.8.3.555.

JGJ 149 (2006), Technical specification for concrete structures with specially shaped columns, China, M.o.H.a.U.-R.D.o., Beijing, China

GB50011 (2010), Code for seismic design of buildings, China, N.S.o.t.P.s.R.o., Beijing, China

Chou, C.C. and Uang, C.M. (2007), "Effects of continuity plate and transverse reinforcement on cyclic behavior of SRC moment connections", *J. Struct. Eng.*, **133**(1), 96-104. https://doi.org/10.1061/(ASCE)0733-9445(2007)133:1(96)5.

Dundar, C. and Sahin, B. (1993), "Arbitrarily shaped reinforced concrete members subject to biaxial bending and axial load", *Comput. Struct.*, **49**(4), 643-662. https://doi.org/10.1016/0045-7949(93)90069-P.

Ghobarah, A., Saatcioglu, M. and Nistor, I. (2006), "The impact of the 26 December 2004 earthquake and tsunami on structures and infrastructure", *Eng. Struct.*, **28**(2), 312-326. https://doi.org/10.1016/j.engstruct.2005.09.028.

Hakuto, S., Park, R. and Tanaka, H. (2000), "Seismic load tests on interior and exterior beam-column joints with substandard reinforcing details", *Struct. J.*, **97**(1), 11-25.

Hsu, C.T.T. (1989), "T-shaped reinforced concrete members under biaxial bending and axial compression", *Struct. J.*, **86**(4), 460-468.

Mahadevappa, P. (1992), "Computer aided analysis of reinforced concrete columns subjected to axial compression and bending—I L-shaped sections", *Comput. Struct.*, **44**(5), 1121-1138. https://doi.org/10.1016/0045-7949(92)90333-U.

Marin, J. (1979). "Design aids for L-shaped reinforced concrete columns", Journal Proceedings.

Mirza, S. and Lacroix, E.A. (2004), "Comparative strength analyses of concrete-encased steel composite columns", *J. Struct. Eng.*, **130**(12), 1941-1953. https://doi.org/10.1061/(ASCE)0733-9445(2004)130:12(1941).

Montava Belda, I., Irles Más, R., Pomares Torres, J.C. and González Sánchez, A. (2019), "Experimental Study of Steel Reinforced Concrete (SRC) Joints", Applied Science.

N,W. (2014), "Research on seismic performance of steel reinforced concrete L-shaped column space corner joint", Ph.D; Guangxi University.

Pan, P., Lin, X., Lam, A., Chen, H. and Ye, L. (2014), "Monotonic loading tests of ring-beam connections for steel reinforced concrete columns and RC beams", *J. Struct. Eng.*, **140**(4), 04013092. https://doi.org/10.1061/(ASCE)ST.1943-541X.0000911.

Pantazopoulou, S.J. and Bonacci, J. (1994), "On earthquake-resistant reinforced concrete frame connections", *Can. J. Civil Eng.*, **21**(2), 307-328. https://doi.org/10.1139/l94-032.

Park, H.G., Hwang, H.J., Lee, C.H., Park, C.H. and Lee, C.N. (2012), "Cyclic loading test for concrete-filled U-shaped steel beam–RC column connections", *Eng. Struct.*, **36**, 325-336. https://doi.org/10.1016/j.engstruct.2011.12.033.

Prota, A., Nanni, A., Manfredi, G. and Cosenza, E. (2004), "Selective upgrade of underdesigned reinforced concrete beam-column joints using carbon fiber-reinforced polymers", *Struct. J.*, **101**(5), 699-707.

Ramamurthy, L. and Khan, T.H. (1983), "L-shaped column design for biaxial eccentricity", *J. Struct. Eng.*, **109**(8), 1903-1917.

Thomas, C.T. and M. ASCE (1985), "Biaxially loaded L-shaped reinforced concrete columns", *J. Struct. Eng.*, **111**(12), 2576-2595. https://doi.org/10.1061/(ASCE)0733-9445(1983)109:8(1903).

Wakabayashi, M. and Minami, K. (1980), "Developments in composite and mixed construction: recent experimental studies on the hysteretic characteristics of beam-to-column connections in composite structures", *Proceedings of the USA–Japan seminar on composite structures and mixed structural systems*.

Wang, W., Chen, Y., Li, W. and Leon, R.T. (2011), "Bidirectional seismic performance of steel beam to circular tubular column connections with outer diaphragm", *Earthq. Eng. Struct. D.*, **40**(10), 1063-1081. https://doi.org/10.1002/eqe.1070.

Wang, Y. (2008), "Lessons learned from the "5.12" Wenchuan Earthquake: evaluation of earthquake performance objectives and the importance of seismic conceptual design principles", *Earthq. Eng. Eng. Vib.*, **7**(3), 255-262. https://doi.org/10.1007/s11803-008-0886-8.

Xiang, P., Deng, Z., Su, Y., Wang, H. and Wan, Y. (2017), "Experimental investigation on joints between steel-reinforced concrete T-shaped column and reinforced concrete beam under bidirectional low-cyclic reversed loading", *Adv. Struct. Eng.*, **20**(3), 446-460. https://doi.org/10.1177/1369433216653841.

Xu, C., Peng, S., Wang, C. and Ma, Z. (2020), "Influence of the degree of damage and confinement materials on the seismic behavior of RC beam-SRC column composite joints", *Compos. Struct.*, **231**, 111002.

https://doi.org/10.1016/j.compstruct.2019.111002.

Xu, J., Chen, Z., Chen, Y. and Xue, J. (2015), "Earthquake damage evaluation of T-shaped SRC composite column-steel beams in 3D connection joints", *Adv. Struct. Eng*., **18**(5), 701-713. https://doi.org/10.1260/1369-4332.18.5.701.

Xue, J., Chen, Z., Zhao, H., Gao, L. and Liu, Z. (2012), "Shear mechanism and bearing capacity calculation on steel reinforced concrete special-shaped columns", *Steel Compos. Struct*., **13**(5), 473-487. https://doi.org/10.12989/scs.2012.13.5.473.

Yang, Y., Wang, Y., Fu, F. and Liu, J. (2015), "Static behavior of T-shaped concrete-filled steel tubular columns subjected to concentric and eccentric compressive loads", *Thin-Wall. Struct*., **95**, 374-388. https://doi.org/10.1016/j.tws.2015.07.009.

Zhao, Y., Li, Z. and Chen, Y. (2004), "Research on limit values of axial compression ratios of specially shaped RC columns in case of 4th aseismic grade", *J. Build. Struct*., **25**(3), 58-62. (in Chinese)

BU